Supervised Classification of Fully PolSAR Images Using Active Contour Models

Daniel Santana-Cedrés, Luis Gomez, *Senior Member, IEEE*, Agustín Trujillo, Miguel Alemán-Flores, Rachid Deriche, Luis Alvarez

***Abstract*—In this paper we propose a supervised method for the classification of Fully PolSAR (Polarimetric Synthetic Aperture Radar) images based on active contour models. We use an "a priori" estimation, obtained from training data, of the complex Wishart distributions of the different types of regions in the image (for instance, water, crops, grass, forest or urban). The information of the Wishart distributions is included in the active contour models to guide the level set evolution. We study the case of 2 classes and the case of 3 or more classes separately. We present some experimental results on synthetic data and real PolSAR images to show the performance of the proposed model. The results are compared to other well-known supervised classification methods and, for actual PolSAR data, our method shows an overall precision of 94.31% and a κ coefficient of 0.937.**

***Index Terms*—Polarimetric synthetic aperture radar (PolSAR) snakes, active contours, classification, statistical learning.**

I. Introduction

FULLY PolSAR (Polarimetric synthetic aperture radar) measures target reflectivity by using four polarization combinations, which provides better scattering measures than monopolarized SAR systems. Due to that, PolSAR is an effective tool to monitor ground surface and to perform terrain and land use classification [1], [2], [3].

Classification methods can be divided into unsupervised methods and supervised methods. Although unsupervised approaches (automatic classification without the intervention of a user) are desirable and strongly pursued [4], due to the complexity of PolSAR data, most practical methods are either semi-supervised or supervised. Supervised methods rely on the use of a reduced set of labeled samples (*training set*), marked by an expert and used to obtain some information and perform the data classification. Some supervised methods for PolSAR classification use statistical information from PolSAR data, such as the Wishart classifier [2], or machine learning techniques, such as support vector machines [5] or random forests [6], showing, in general, excellent performances. Classification by using deep neural convolution networks constitutes an active area of research on supervised methods, providing results for PolSAR classification comparable to state-of-the art techniques [7].

Manuscript received ***, ****; revised ***, ****.

D. Santana-Cedrés, L. Gomez, A. Trujillo, M. Alemán-Flores, and L. Alvarez are with the Imaging Technology Center (CTIM), University of Las Palmas de Gran Canaria, Spain, email: dsantana@ctim.es, {luis.gomez, agustin.trujillo, miguel.aleman, lalvarez}@ulpgc.es

R. Deriche is with Athena Project-Team, Inria Sophia Antipolis Méditerannée, France. Email: rachid.deriche@inria.fr

In this paper we address the problem of supervised PolSAR image classification using active contour models. Although some works using active contours have been published for SAR and PolSAR data [8], they focus on image segmentation and not on image classification.

The classical geodesic active contours [9] allow adjusting an initial approximation of a contour to the most significant edges in the surrounding region. Active contour models including statistical information have also been proposed in [10], [11]. For each pixel in the image domain, the PolSAR image provides a Hermitian positive matrix. Moreover, within each class of the image (given by the type of region: water, crops, grass, forest, urban, etc.), the Hermitian positive matrices follow a complex Wishart distribution. Due to these special characteristics of the PolSAR images, the extension of the usual active contour models to PolSAR images is not trivial. The main contribution of this paper is a new formulation of the active contour model, adapted to the features of PolSAR images, which includes estimations of the Wishart models in each class obtained from training data.

The rest of the paper is organized in the following way: in Section 2, we present a brief introduction to the Wishart distribution used as statistical model of the PolSAR image distribution, as well as a robust technique for the estimation of the Wishart parameters of each class. In Section 3, we introduce the active contour models proposed to perform a supervised region classification. Section 4 shows some experimental results on synthetic and real PolSAR images. Finally, in Section 5, we present some conclusions.

II. The Complex Wishart distribution

A. Characterization

This section is based on the work by Nascimento et al. [12]. The polarimetric coherent information associates to each pixel, and for each frequency of operation, a 2×2 complex matrix with entries S_{VV}, S_{VH}, S_{HV}, and S_{HH}, where S_{ij} is the backscattered signal for the ith transmission and jth reception linear polarization, $i,j = \mathrm{H},\mathrm{V}$. Under the conditions of reflection symmetry, $S_{\mathrm{HV}} = S_{\mathrm{VH}}$, and the scattering matrix can be simplified as the three-component complex vector $\boldsymbol{s} = \begin{bmatrix} S_{\mathrm{VV}} & \sqrt{2}\,S_{\mathrm{VH}} & S_{\mathrm{HH}} \end{bmatrix}^{\top}$, where $^{\top}$ denotes vector transposition. This random vector can be modeled by the zero-mean multivariate complex Gaussian distribution [13].

Different targets are characterized by different variances. In the area covered by each image pixel, L independent measurements of the same target are obtained while processing the raw

data. This quantity is the number of looks. These observations are used to produce the "multilook sample covariance matrix"

$$\boldsymbol{Z} = \frac{1}{L}\sum_{i=1}^{L} \boldsymbol{s}_i \boldsymbol{s}_i^*, \tag{1}$$

where the superscript $*$ represents the complex conjugate transpose of a vector, and $\boldsymbol{s}_i$, $i = 1, 2, \ldots, L$, are the L scattering vectors. Assuming that these vectors are independent, $\boldsymbol{Z}$ is a Hermitian positive definite matrix and follows a scaled complex Wishart distribution [14]. Having $\boldsymbol{\Sigma}$ and L as parameters, the scaled complex Wishart distribution is characterized by the following probability density function

$$f_{\boldsymbol{Z}}(\boldsymbol{z}; \boldsymbol{\Sigma}, L) = \frac{L^{3L}|\boldsymbol{z}|^{L-3}}{|\boldsymbol{\Sigma}|^{L}\Gamma_3(L)} \exp\big(-L\,\mathrm{tr}(\boldsymbol{\Sigma}^{-1}\boldsymbol{z})\big), \tag{2}$$

where $\Gamma_3(L) = \pi^3 \prod_{i=0}^{2}\Gamma(L-i)$ for $L \geq 3$, $\Gamma(\cdot)$ is the gamma function, $\mathrm{tr}(\cdot)$ represents the trace operator, $|\cdot|$ denotes the determinant operator, $\boldsymbol{\Sigma}$ is the covariance matrix associated to $\boldsymbol{s}$, $\Sigma = \mathrm{E}\big(\boldsymbol{s}\boldsymbol{s}^*\big)$, where $\mathrm{E}(\cdot)$ is the expectation. The first moment of $\boldsymbol{Z}$ satisfies $\mathrm{E}(\boldsymbol{Z}) = \boldsymbol{\Sigma}$. We denote $\boldsymbol{Z} \sim \mathcal{W}(\boldsymbol{\Sigma}, L)$ to indicate that $\boldsymbol{Z}$ follows the complex Wishart distribution. As observed in [15], this distribution is able to accommodate an arbitrary number of polarimetric components.

B. Robust Supervised Parameter Estimation

We assume that the PolSAR image pixels can be separated in N_c classes corresponding to different types of regions and that the image values in such regions follow a Wishart distribution $\mathcal{W}(\boldsymbol{\Sigma_m}, L)$ with $m = 1, .., N_c$. We also assume that the number of looks, L, is known "a priori" and is the same for all classes. To estimate the covariance matrix $\boldsymbol{\Sigma_m}$, we use a supervised learning procedure. For each class, we manually select a region of pixels belonging to the target class and we assume that the PolSAR image values $\{\boldsymbol{\Sigma}_m^1, \boldsymbol{\Sigma}_m^2, \ldots, \boldsymbol{\Sigma}_m^{N_m}\}$ are random samples of $\mathcal{W}(\boldsymbol{\Sigma_m}, L)$. Frery et al. [16] showed that the ML estimator for $\boldsymbol{\Sigma_m}$ is a quantity that maximizes the log-likelihood function associated to the Wishart distribution given by the sample mean

$$\widehat{\boldsymbol{\Sigma}}_{\mathrm{ML}}^m = \overline{\boldsymbol{\Sigma}_m} = \frac{\Sigma_{k=1}^{k=N_m}\boldsymbol{\Sigma}_m^k}{N_m}, \tag{3}$$

so that using this approach we obtain an estimation of $\boldsymbol{\Sigma_m}$.

In general, real PolSAR images are corrupted by speckle noise, and the manually selected regions to compute the class representative $\boldsymbol{\Sigma_m}$ include outliers which might have a strong influence on the estimation. In this paper we propose a technique to remove outliers in the estimation of $\boldsymbol{\Sigma_m}$ based on the Kullback-Leibler (KL) stochastic distance given by:

$$d_{\mathrm{KL}}\left(\boldsymbol{\Sigma_1}, \boldsymbol{\Sigma_2}\right) = L\left[\frac{\mathrm{tr}\left(\boldsymbol{\Sigma_1}^{-1}\boldsymbol{\Sigma_2} + \boldsymbol{\Sigma_2}^{-1}\boldsymbol{\Sigma_1}\right)}{2} - 3\right]. \tag{4}$$

First, we compute the mean, in the sense of the Kullback-Leibler distance, of the sequence $\{\boldsymbol{\Sigma}_m^1, \boldsymbol{\Sigma}_m^2, \ldots, \boldsymbol{\Sigma}_m^{N_m}\}$, which is given by the expression

$$\widehat{\boldsymbol{\Sigma}}_{\mathrm{KL}}^m = \sqrt{\mathbf{B_m^{-1}}}\left[\sqrt{\sqrt{\mathbf{B_m}}\mathbf{A_m}\sqrt{\mathbf{B_m}}}\right]\sqrt{\mathbf{B_m^{-1}}}, \tag{5}$$

where $\mathbf{A_m} = \overline{\boldsymbol{\Sigma_m}}$ and $\mathbf{B_m} = \overline{(\boldsymbol{\Sigma_m})^{-1}}$. Indeed, Wang et al. showed in [17] that the above matrix satisfies

$$\widehat{\boldsymbol{\Sigma}}_{\mathrm{KL}}^m = \arg\min_{\boldsymbol{\Sigma}} \frac{\Sigma_{k=1}^{k=N_m} d_{\mathrm{KL}}\left(\boldsymbol{\Sigma}, \boldsymbol{\Sigma}_m^k\right)}{N_m}. \tag{6}$$

Originally, they showed this result for real symmetric positive matrices, but we can easily check that it is also true for complex Hermitian positive matrices. Next, to remove outliers, we compute the $90th$ percentile, P_{90}, of $\{d_{\mathrm{KL}}\left(\widehat{\boldsymbol{\Sigma}}_{\mathrm{KL}}^m, \boldsymbol{\Sigma}_m^k\right)\}_{k=1,..,N_m}$ and we remove from the sequence any matrix $\boldsymbol{\Sigma}_m^k$ satisfying $d_{\mathrm{KL}}\left(\widehat{\boldsymbol{\Sigma}}_{\mathrm{KL}}^m, \boldsymbol{\Sigma}_m^k\right) > 2P_{90}$. Once the outliers have been removed, we recompute the class representative $\widehat{\boldsymbol{\Sigma}}_{\mathrm{KL}}^m$ using equation (5). We repeat this procedure iteratively until no more outliers are removed. In other words, we stop the procedure when, for any k, $d_{\mathrm{KL}}\left(\widehat{\boldsymbol{\Sigma}}_{\mathrm{KL}}^m, \boldsymbol{\Sigma}_m^k\right) \leq 2P_{90}$ (figures about this procedure are included in Table I).

III. Active Contour Models

A. Two-Class Level Set Formulation

The classical formulation of the active contour technique aims to adapt an initial contour, Γ_0, in such a way that it moves locally toward the highest gradients, but preserving a certain degree of smoothness. Therefore, it usually consists of two terms which compete to reach a balance between contrast and regularity. The level set formulation of the geodesic active contours (GAC) described in [9] is given by

$$\frac{\partial u}{\partial t} = g\left(I\right)\mathrm{div}\left(\frac{\nabla u}{\|\nabla u\|}\right)\|\nabla u\| + \nabla u \cdot \nabla g\left(I\right), \tag{7}$$

where $\Gamma_t = \partial\{(x, y) : u(t, x, y) > 0\}$ is an implicit representation of the evolution of the optimized contour, I is the image on which the segmentation is performed and $g(.)$ acts as an edge stopping function which satisfies that $g(I)(x, y)$ is small in the pixels (x, y) where $I(x, y)$ has a high gradient magnitude. Usually, Γ_0 is given as the boundary of a set Ω_0 (the initial segmentation) and $u_0(x, y)$ is chosen as the signed distance function $d_{\Omega_0}(x, y)$. In [18] the following extension of this equation, including a histogram-based term, is proposed in the context of medical image segmentation

$$\frac{\partial u}{\partial t} = g(I)div\left(\frac{\nabla u}{\|\nabla u\|}\right)\|\nabla u\| + \nabla g(I)\cdot\nabla u + \alpha k(I)\|\nabla u\|, \tag{8}$$

where $\alpha \geq 0$ is a parameter to balance the weight of the new term. The forcing term $k(I)$ includes statistical information about the image intensity. In [19] a mathematical study of this type of equation with a forcing term is presented.

To extend this active contour model to PolSAR images, we have to adapt the edge stopping function $g(I)(x, y)$ and the forcing term $k(I)(x, y)$. The structure tensor, [20], has been extensively used to analyze the local behavior of scalar images. To extend $g(I)(x, y)$, we use the following generalization of the structure tensor to PolSAR images introduced in [21]. First,

for $n, m \in \{-h, 0, h\}$ (where h is the interpixel distance) and (x, y) an image point, we define

$$d_\sigma^{n,m}(x,y) = d_{\mathrm{KL}}(I_\sigma(x+n, y+m), I_\sigma(x-n, y-m)), \quad (9)$$

where I_σ represents the convolution of the original PolSAR image with a Gaussian kernel K_σ. Then we define the generalization of the structure tensor matrix as

$$J_\rho(I_\sigma) \equiv K_\rho * \begin{pmatrix} \left(d_\sigma^{1,0}\right)^2 & sgn(s) d_\sigma^{1,0} d_\sigma^{0,1} \\ sgn(s) d_\sigma^{1,0} d_\sigma^{0,1} & \left(d_\sigma^{0,1}\right)^2 \end{pmatrix} \quad (10)$$

where $s(x,y) = d_\sigma^{1,1}(x,y) - d_\sigma^{1,-1}(x,y)$ and $sgn(.)$ is the signum function. The maximum eigenvalue of this matrix $\lambda_{max}(J_\rho(I_\sigma))(x,y)$ measures the variability of the PolSAR image in a neighborhood of the point (x,y). The main advantage with respect to other extensions of the structure tensor of vector-valued images is that the one we propose is adapted to PolSAR images and uses the stochastic Kullback-Leibler distance to measure the image variability. Next, we define $g(I)$ as

$$g(I)(x,y) = \frac{1}{1 + c \cdot \lambda_{max}(J_\rho(I_\sigma))(x,y)}, \quad (11)$$

where $c \geq 0$.

To define the extension of the forcing term $k(I)$ to PolSAR images we use the estimation of the Wishart distribution $\mathcal{W}(\mathbf{\Sigma_m}, L)$ for each class $m = 1, 2$ and we define $k(I)$ as

$$k(I)(x,y) = log\left(\frac{\epsilon + f_{\boldsymbol{Z}}(I(x,y); \mathbf{\Sigma_1}, L)}{\epsilon + f_{\boldsymbol{Z}}(I(x,y); \mathbf{\Sigma_2}, L)}\right), \quad (12)$$

where $\epsilon > 0$ is introduced to avoid singularities in the above expression in case $f_{\boldsymbol{Z}}(I(x,y); \mathbf{\Sigma_2}, L)$ is close to zero. We point out that, if, for a covariance matrix $I(x,y)$, the Wishart probability density function evaluated in $I(x,y)$ is higher for class 1 than for class 2, then $k(I)(x,y)$ is positive, and negative otherwise. Moreover, the higher the disparity between both probabilities, the greater the magnitude of k, which means that the ambiguity is lower. This function can be used to guide the contour in such a way that it inflates or deflates automatically toward the surrounding regions which are more likely to be in the first region.

B. Multi-class Level Set Formulation

In the general case, we deal with N_c classes, and the level set formulation is given by the vector-valued function $u(t,x,y) = \{u^m(t,x,y)\}_{m=1,..,N_c}$. For any $t \geq 0$, $u(t,x,y)$ generates a partition of the image domain Ω iff

$$H_u(t,x,y) \equiv 1 - \sum_{m=1}^{N_c} H(u^m(t,x,y)) = 0 \quad (13)$$

where $H(.)$ is the Heaviside step function. In other words, $\{u^m(t,x,y)\}$ generates a partition of Ω iff, for any $t \geq 0$ and $(x,y) \in \Omega$, there exists a unique $m_0 \in \{1,..,N_c\}$ such that $u^{m_0}(t,x,y) \geq 0$. The multi-class level formulation we propose is given by the following differential equation system:

$$\frac{\partial u^m}{\partial t} = g(I) div\left(\frac{\nabla u^m}{\|\nabla u^m\|}\right)\|\nabla u^m\| + \nabla g(I) \nabla u^m + (\alpha \cdot k^m(I) + \beta \cdot H_u)\|\nabla u^m\|, \quad (14)$$

where $\beta \geq 0$. The edge stopping function $g(I)$, given by the generalization of the structure tensor, is the same for all equations, and $k^m(I)$ is a forcing term given by

$$k(I)^m(x,y) = log\left(\frac{\epsilon + f_{\boldsymbol{Z}}(I(x,y); \mathbf{\Sigma_m}, L)}{\epsilon + sup_{j \neq m} f_{\boldsymbol{Z}}(I(x,y); \mathbf{\Sigma_j}, L)}\right). \quad (15)$$

The introduction of the function H_u in equation (15) creates a dependence between all components of $u(t,x,y)$. Indeed, if $H_u(t,x,y) < 0$, more than one component is positive and then all components tend to decrease until only one is positive in the point. On the other hand, in the case $H_u(t,x,y) > 0$ for all components, all of them tend to increase until one of the components u^m becomes positive. In [22], [23], similar multi-class level set formulations are introduced for scalar and vector-valued images. The initial guess $u_0^m(x,y)$ is chosen as the signed distance function $d_{\Omega_0^m}(x,y)$, where

$$\Omega_0^m = \{(x,y) : \ k(I)^m(x,y) \geq 0\}. \quad (16)$$

Once the solution $u(t,x,y)$ of the PDE system becomes stable, we classify the points (x,y) of the image domain in the following way:

$$(x,y) \in \text{ class } m \text{ if } \forall j \neq m \ u^m(t,x,y) \geq u^j(t,x,y). \quad (17)$$

IV. Results and Discussion

To validate our proposal, we performed experiments using both synthetic and real PolSAR data. In both cases, ground-truth images have been provided in order to assess the accuracy. The results were compared with well-known supervised methods. For all the techniques included in the comparison, the class representatives were computed by randomly selecting 50% of each ground-truth class, preserving the other half for validation purposes.

Polarimetric synthetic data (*phantom*) of size 500×500 pixels were generated from samples belonging to actual PolSAR data to have a ground truth to compare the results with. The phantom has large homogeneous areas for classification purposes and also several rectangles of different sizes to evaluate the preservation of the edges (see Fig. 1).

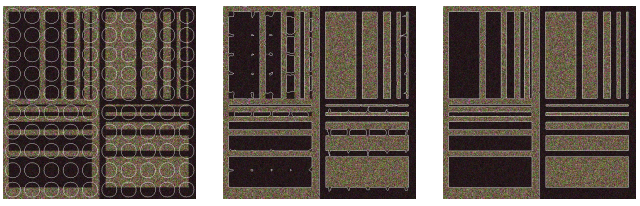

(a) $t = 0$ (b) $t = 240$ (c) $t = 800$

Fig. 1. Illustration of a collection of contours and their evolution using the active contour model (see video at this link)

Figure 1 shows different instants in the evolution of the contours on the phantom image. From the initialization of the contours as circles (Fig. 1(a)) until the end of the process (Fig. 1(c)), the contours tend to adjust to the different classes, until their complete separation, preserving the edges in all the cases. Quantitatively, and regarding the segmentation of two classes,

the method achieves an overall precision of 99.62%. Note that these data have not been pre-filtered.

For the multi-class case, we carried out experiments with real data. To this purpose, we have used a well-known 4-look 1024×750-pixel PolSAR image belonging to the region of Flevoland in the Netherlands (available at ESA sample datasets - Fig. 2(a)). The result of the edge stopping function with $\lambda = 5$ is shown in Fig. 2(b). As observed, most of the contours which define the different regions are highlighted, and hence, correctly detected.

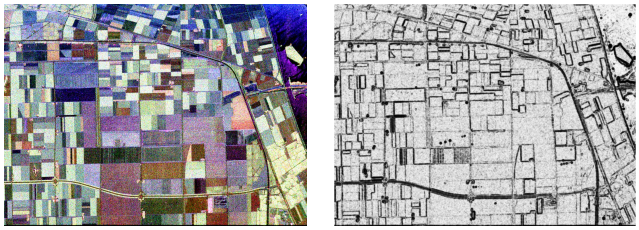

(a) Pauli representation (b) $g(I)(x, y)$

Fig. 2. Flevoland PolSAR image: (a) Pauli codification and (b) representation of the edge stopping function $g(I)(x, y)$ with $\lambda = 5$

As in the case of the phantom data a ground truth was manually generated for the real sequence, partially based on [24]. In Fig. 3, this ground truth is shown, including the 14 different classes which were labeled. It has been obtained by applying the preprocessing step described in section II-B. This ground truth was also used with the other compared methods.

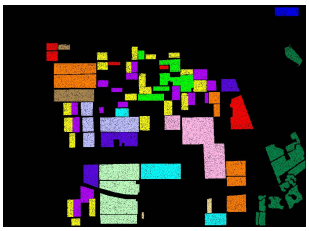

Fig. 3. Ground truth provided for the real PolSAR image of Flevoland: steam beans, bare soil, rapeseed, potatoes, beet, wheat B, peas, wheat C, lucerne, grass, building, wheat A, forest, and water

Since we are dealing with a multi-class scenario, instead of initializing the contours by using circles, the pre-classification result provided by the Wishart distribution is used to purvey an initialization to guide the evolution of the multi-class level sets. Although the proposed method does not include a despeckling filter, the extended Lee filter [25] for covariance matrices was used to reduce speckle noise from the input data provided to the rest of the applied techniques, in order to perform a fair comparison with our proposal, which includes a regularization term.

Fig. 4 shows the classification by maximum likelihood by using the Wishart distribution (Fig. 4(a)), the stochastic Hellinger distance (Fig. 4(b)), K-means (Fig. 4(c)), and the PolSAR active contours (Fig. 4(d)). As observed, the Wishart, Hellinger and K-Means classifiers are not able to separate the classes completely. They include small isolated areas labeled

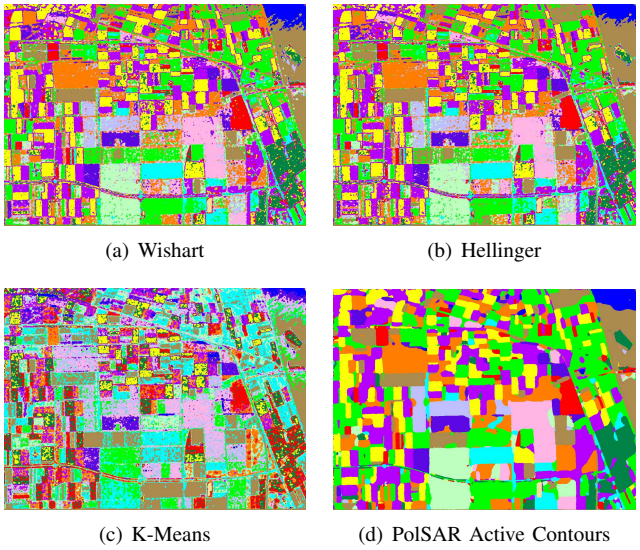

(a) Wishart (b) Hellinger

(c) K-Means (d) PolSAR Active Contours

Fig. 4. Results of applying different classification techniques: (a) Wishart, (b) Hellinger, (c) K-Means, and (d) PolSAR active contours

as belonging to other classes, in spite of the fact that a despeckling filter has been used. In addition, some regions are almost completely misclassified, as in the case of the rapeseed or wheat B classes in the K-Means technique. The PolSAR active contour approach is able to classify the data in a much better way, showing uniform regions without small isolated spots.

On the other hand, quantitative results for the different classifiers are included in table I. Note that, in order to obtain such percentages, only the pixels not included in the computation of the representatives are considered. In each row, the precision for the different classes is indicated and, at the bottom of the table, the overall precision (OP) and the kappa coefficient (κ) is included. As can be observed, for most of the classes, the proposed method outperforms the rest of the techniques, obtaining percentages over 90%. Only in the case of bare soil, the obtained accuracy is lower than in the other methods. In fact, it is quite natural that the method performs comparatively worse for bare-soil because the points inside areas with low crop density are likely to be misclassified as bare soil. In the case of rapeseed, grass or forest, the active contour approach obtains percentages which are significantly higher than for the rest of the methods. The proposed approach improves the overall precision of the other methods by 10% to 25%. Regarding the kappa coefficient, the value obtained by applying the active contours improves notably the results provided by the Wishart, Hellinger, and K-Means techniques. Although our approach is computationally slower, the computational time is still reasonable and the results are qualitatively and quantitatively superior.

V. Conclusion

A supervised method for Fully PolSAR classification based on active contour models has been presented. Firstly, to identify two classes, a formulation based on the geodesic active contours, which includes an extension of this model

TABLE I
COMPARATIVE RESULTS FOR FLEVOLAND POLSAR IMAGE

Classes	Outliers Removing		Methods (%)			
	Before	After	Wishart	Hellinger	K-Means	PolSAR A.C.
Stem Beans	2320	1934	88.74	87.89	78.02	**97.48**
Bare Soil	9056	7941	93.54	**95.27**	90.07	86.60
Rapeseed	6376	5540	69.22	69.03	40.54	**99.13**
Potatoes	20621	17494	83.62	81.51	64.13	**91.72**
Beet	21442	17794	83.19	84.60	73.84	**93.44**
Wheat B	10283	9096	81.71	81.47	59.01	**96.85**
Peas	14883	13348	90.98	86.90	73.94	**98.72**
Wheat C	22863	20571	85.34	87.49	78.49	**99.04**
Lucerne	11248	10000	92.61	92.47	90.14	**98.67**
Grass	11954	10781	78.94	78.14	60.66	**95.12**
Building	11200	10097	90.79	82.86	67.01	**92.05**
Wheat A	20625	18708	82.65	79.58	67.24	**86.35**
Forest	23438	21364	86.13	84.00	72.97	**98.89**
Water	962	781	99.90	99.69	71.46	**100.00**
OP			83.57	82.72	68.41	**94.31**
κ			0.819	0.811	0.653	**0.937**
Time (sec)			62.99	71.36	27.32	237.78

to PolSAR images, has been introduced by redefining the stopping function and the forcing term. Secondly, an extension to multi-class classification is presented, were the Heaviside step function is included to create a dependence between all the components.

It is worth noting that the ground-truth data, widely used and obtained from different sources, do not consider the presence of outliers inside the labeled regions. In this regard, a preprocessing step to remove them, based on the Kullback-Leibler (KL) stochastic distance, has been proposed.

We have performed experiments on both, synthetic and real data, in order to test the accuracy when detecting two or more classes in PolSAR images. We have presented a comparison with other well-known supervised techniques. Such techniques are applied on filtered input images, in order to perform a fair comparison with the active contours. Qualitatively, the proposed approach obtains better results, by identifying regions which are more uniform in comparison with the other methods. Quantitatively, the application of this generalization of the active contours to PolSAR images produces significantly better results for all but one class, improving considerably the overall precision and the κ coefficient as well.

ACKNOWLEDGMENT

This research has partially been supported by the MINECO project MTM2016-75339-P (Ministerio de Economía y Competitividad, Spain).

REFERENCES

[1] A. Freeman and S. L. Durden, "A three-component scattering model for polarimetric SAR data," *IEEE Trans. Geosci. Remote Sens.*, vol. 36, no. 3, pp. 963–973, May 1998.

[2] L. Gomez, L. Alvarez, L. Mazorra, and A. C. Frery, "Classification of complex Wishart matrices with a diffusion-reaction system guided by stochastic distances," *Philosophical Transactions of The Royal Society A*, vol. 373, no. 2056, pp. 1–14, 2015.

[3] W. Xie, L. Jiao, and J. Zhao, "PolSAR image classification via D-KSVD and NSCT-Domain features extraction," *IEEE Trans. Geosci. Remote Sens.*, vol. 13, no. 2, pp. 227–231, Feb. 2016.

[4] D. Ratha, A. Bhattacharya, and A. C. Frery, "Unsupervised classification of PolSAR data using a scattering similarity measure derived from a geodesic distance," *IEEE Geosci. Remote Sens. Lett.*, vol. 15, no. 1, pp. 151–155, 2018.

[5] S. Alim, P. Gamba, P. Du, and J. Luo, "Active extreme learning machines for quad-polarimetric SAR imagery classification," *International Journal of Applied Earth Observation and Geoinformation*, vol. 35, pp. 305–319, Mar. 2015.

[6] R. Hansch and O. Hellwich, "Evaluation of tree creation methods within random forests for classification of PolSAR images," 2015, pp. 361–364, IGARSS 2015.

[7] Y. Zhou, H. Wang, F. Xu, and Y.-Q. Jin, "Polarimetric SAR image classification using deep convolutional neural networks," *IEEE Geosci. Remote Sens. Lett.*, vol. 13, no. 12, pp. 1935–1939, 2016.

[8] I. B. Ayed, A. Mitiche, and Z. Belhadj, "Polartimetric image segmentation via maximum-likelihood approximation and efficient multiphase level-sets," *IEEE Trans. Pattern Anal. Mach. Intell.*, vol. 28, no. 9, pp. 1493–1500, 2006.

[9] V. Caselles, R. Kimmel, and G. Sapiro, "Geodesic active contours," *International Journal of Computer Vision*, vol. 22, no. 1, pp. 61–79, Feb 1997.

[10] C. Lenglet, M. Rousson, and R. Deriche, "Segmentation of 3d probability density fields by surface evolution: Application to diffusion mri," *Lecture Notes in Computer Science*, vol. 3216, no. PART 1, pp. 18–25, 12 2004.

[11] D. Cremers, M. Rousson, and R. Deriche, "A review of statistical approaches to level set segmentation: Integrating color, texture, motion and shape," *International Journal of Computer Vision*, vol. 72, no. 2, pp. 195–215, Apr 2007.

[12] A. D. Nascimento, A. C. Frery, and R. J. Cintra, "Bias correction and modified profile likelihood under the wishart complex distribution," *IEEE Trans. Geosci. Remote Sens.*, vol. 52, no. 8, pp. 4932–4941, 2014.

[13] N. Goodman, "The distribution of the determinant of a complex Wishart distributed matrix," *The Annals of mathematical statistics*, vol. 34, no. 1, pp. 178–180, 1963.

[14] S. N. Anfinsen, A. P. Doulgeris, and T. Eltoft, "Estimation of the equivalent number of looks in polarimetric synthetic aperture radar imagery," *IEEE Trans. Geosci. Remote Sens.*, vol. 47, no. 11, pp. 3795–3809, Nov 2009.

[15] A. C. Frery, A. D. Nascimento, and R. J. Cintra, "Analytic expressions for stochastic distances between relaxed complex Wishart distributions," *IEEE Trans. Geosci. Remote Sens.*, vol. 52, no. 2, pp. 1213–1226, 2014.

[16] A. C. Frery, R. J. Cintra, and A. D. C. Nascimento, "Entropy-based statistical analysis of PolSAR data," *IEEE Trans. Geosci. Remote Sens.*, vol. 51, no. 6, pp. 3733–3743, June 2013.

[17] Z. Wang and B. C. Vemuri, "An affine invariant tensor dissimilarity measure and its applications to tensor-valued image segmentation," in *Proc. IEEE Comput. Soc. Conf. on Comput. Vis. and Pattern. Recognit., 2004. CVPR 2004.*, vol. 1, June 2004, pp. I–228–I–233 Vol.1.

[18] M. Alemán-Flores, D. Santana-Cedrés, L. Alvarez, A. Trujillo, L. Gomez, P. G. Tahoces, and J. M. Carreira, "Segmentation of the aorta using active contours with histogram-based descriptors," in *MICCAI Workshop LABELS-CVII-STENT*, vol. LNCS 11043, 2018, pp. 28–35.

[19] L. Alvarez, C. Cuenca, J. Díaz, and E. González, "Level set regularization using geometric flows," *SIAM Journal on Imaging Sciences*, vol. 11, no. 2, pp. 1493–1523, 2018.

[20] J. Weickert, "Coherence-enhancing diffusion filtering," *International Journal of Computer Vision*, vol. 31, no. 2, pp. 111–127, 1999.

[21] L. Gomez, L. Alvarez, and A. C. Frery, "Local edginess measures in PolSAR imagery by using stochastic distances," 2018, pp. 5800–5803, IGARSS 2018.

[22] N. Paragios and R. Deriche, "Geodesic active regions: A new framework to deal with frame partition problems in computer vision," *Journal of Visual Communication and Image Representation*, vol. 13, no. 1, pp. 249 – 268, 2002.

[23] M. Rousson and R. Deriche, "A variational framework for active and adaptative segmentation of vector valued images," in *Workshop on Motion and Video Computing, 2002. Proceedings.*, 2002, pp. 56–61.

[24] S. Uhlmann and S. Kiranyaz, "Integrating color features in polarimetric sar image classification," *IEEE Trans. Geosci. Remote Sens.*, vol. 52, no. 4, pp. 2197–2216, 2014.

[25] J.-S. Lee and E. Pottier, *Polarimetric radar imaging: from basics to applications*. Boca Raton (FL), USA: CRC press, 2009.